Supplement of

Measurement report: Characterization of uncertainties of fluxes and fuel sulfur content from ship emissions at the Baltic Sea

Jari Walden et al.

Correspondence to: Jari Walden (jari.a.walden@gmail.com)

Uncertainty estimates of the fluxes

The uncertainty estimates of the results for the fluxes measured by the gradient technique and for the FSC are presented in more detail here. Following the procedure by JCGM (JCGM 2008), each of the uncertainty sources in the measurement system that contributes to the dispersion of the measurement results needs to be characterized. In case of the gradient technique, the flux is described by Eq. (5), and the uncertainty of the measurement result is described by Eq. (11). Single standard uncertainties that are considered to contribute to the uncertainty of the flux measurement result are the friction velocity $u*$, the integral of the dimensionless potential function Ψ_c, the measurement height z, and the uncertainty of the measured concentrations of gases and particles. A more detailed description of the sources of errors is found in the literature (Businger, 1986). Of additional sources, nonstationarity, was only partly considered here, whereas errors that flow distortion introduces in the measurement height and the wind speed were corrected. On the other hand, the chemically reactive species NO, $O_{3,}$ and NO_2 were not considered in detail since the concentration difference between the two measurement heights did not exceed the uncertainty limit calculated for these compounds (Fig. S3). Eq. (11) was applied to each of the uncertainty sources in Eq. (5), resulting in an equation that includes a weighting factor and the standard uncertainty of each of the uncertainty sources. The weighing factors were calculated from the measurement results, and each of the uncertainty sources were estimated by the standard deviation of the results or by other means, e.g. by the performance characteristics of the measurement instrument (analyzers etc.). Uncertainties of the analyzers for gaseous compounds and particles were based on the performance characteristics of the analyzers themselves. In case of the analyzers that measure the concentration of ozone, nitrogen oxides and sulfur dioxide, (APOA-370 2006, Environnemet AC31M 2006, Thermo 43i 2006) a complete test report showing the performance characteristics that influence the measurement results has been prepared and made available by the Immissionsschutz und Energiesysteme GmbH, TÜV, (www.qal1.de). Modifications in the complete procedure defined by TÜV were made to fit for the purpose of the measurements conducted at Harmaja. Concerning the CO_2 measurements, the performance of the Licor 7000 and Picarro G2301 analyzers were obtained from the document of the WMO/GAW guidelines (WMO 2013). In case of the particle measurements, the performance of the two ELPI instruments, i.e. ELPI1 and ELPI2, was tested during the measurements by injecting the same air sample into both instruments at certain time frames and at different particle concentrations. The effective variance regression line between the two ELPI instruments (assuming that both instruments have the same statistical uncertainty) was used to correct the results of the ELPI2 with respect to the ELPI1. The corrections have been performed for each of the ELPI2 channels. The scatter of the results of ELPI1 and ELPI2 against each other was obtained by applying orthogonal regression analysis. The scatter of the results represents the uncertainty of the instruments with respect to each other, shown in Fig. S1. This strategy was different from that of the gaseous compounds, for which actual uncertainties of the analyzer results have been obtained. In Fig. S2, the expanded uncertainty of each analyzer is presented as a function of concentration. The differences in the concentrations of the gaseous compounds and number concentrations of nanoparticles from the measurement heights are presented in Fig. S3 together with the uncertainty of the analyzers. Once the difference of the concentrations exceeds the uncertainty limit, the difference is acceptable; otherwise, there is no detectable concentration difference and these measurement results were eliminated. In Fig. S4 the fluxes of CO_2 (mg/m^{2}s) and N_{tot} (counts/m^{2}s) by the gradient technique are presented in the wind sector between 150° and 270°, and with codes 1 and 2 together with their uncertainties. All the uncertainty sources for the flux measurements by the gradient technique are presented in Table S1. The contribution of the friction velocity is obtained from the uncertainty analysis for the EC method since it was taken from the sonic measurements. Two meteorological situations were included: stationary and prevailing situations over the measurement period. The prevailing meteorological situations gives a major contribution to the uncertainty budget while contribution of stationary meteorology is not large.

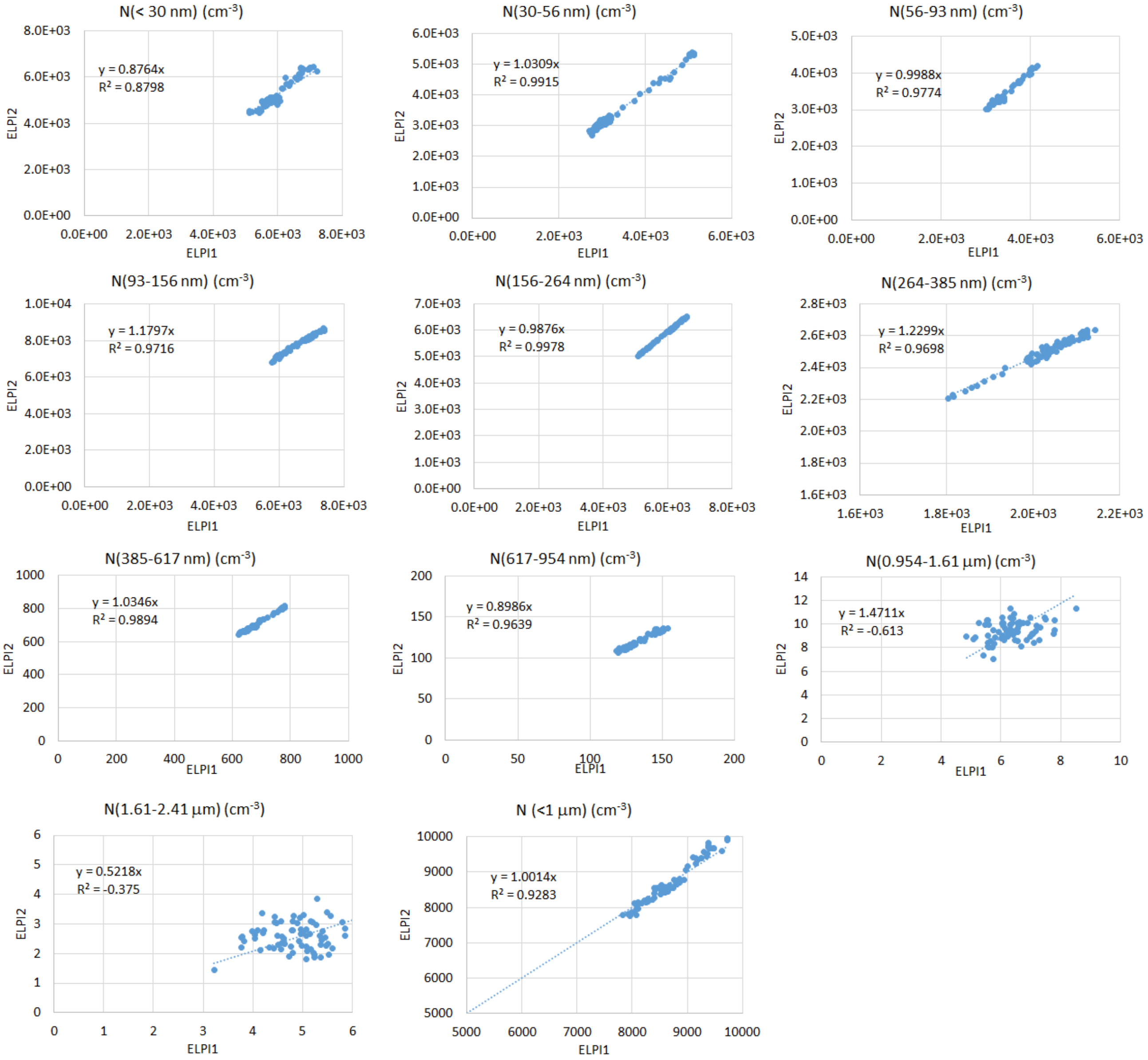

Figure S1. Effective variance regression analysis between the two ELPI instruments at different size classes and different particle concentrations.

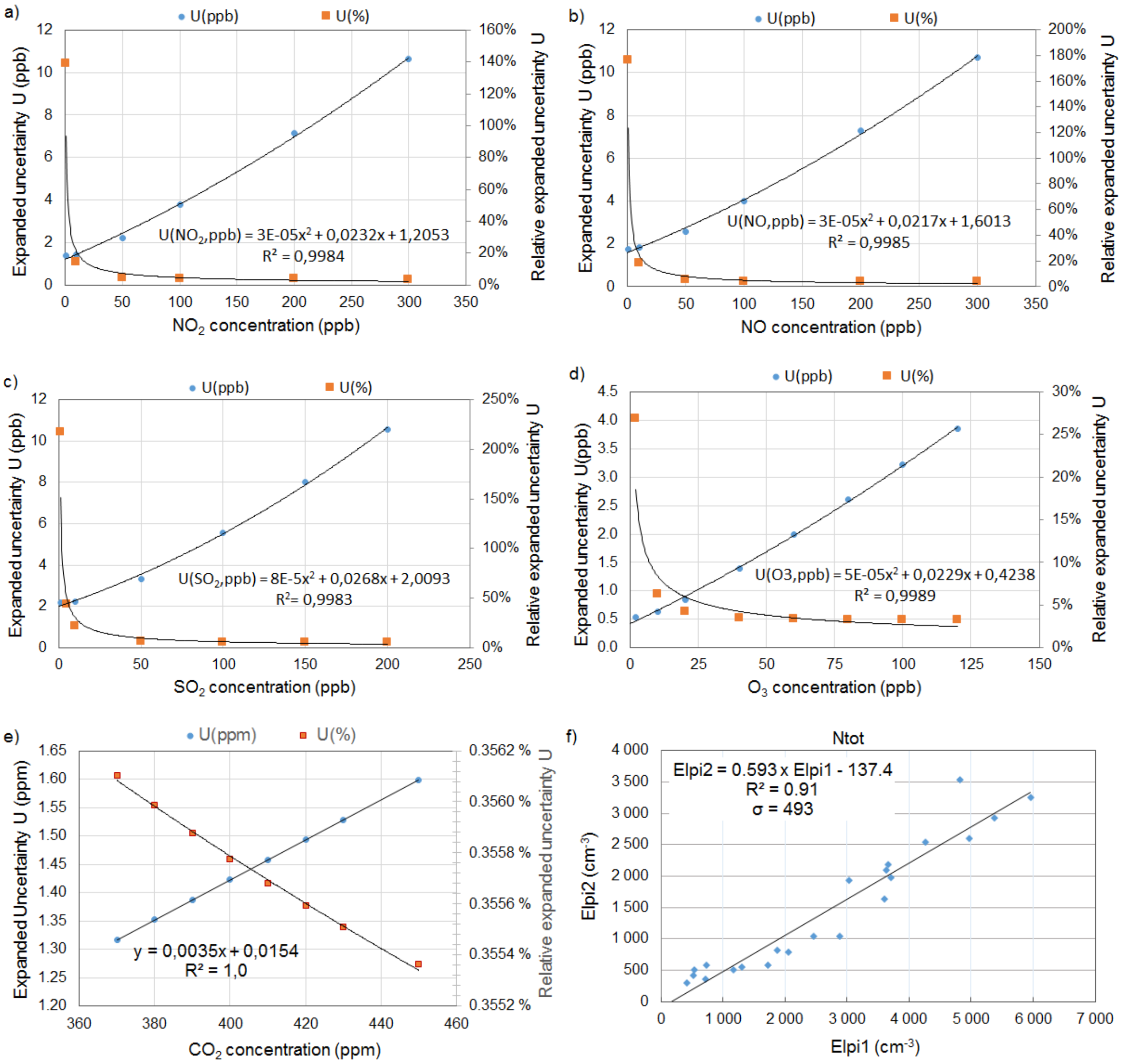

Figure S2. Uncertainty of the measurement results for gaseous compounds and particle number concentration. Figures 2a to 2e represents NO_2-, NO-, SO_2-, O_3- and CO_2-measurements while 2f represents relationship between two particle measurement instrument with standard error of the estimate (σ = 493).

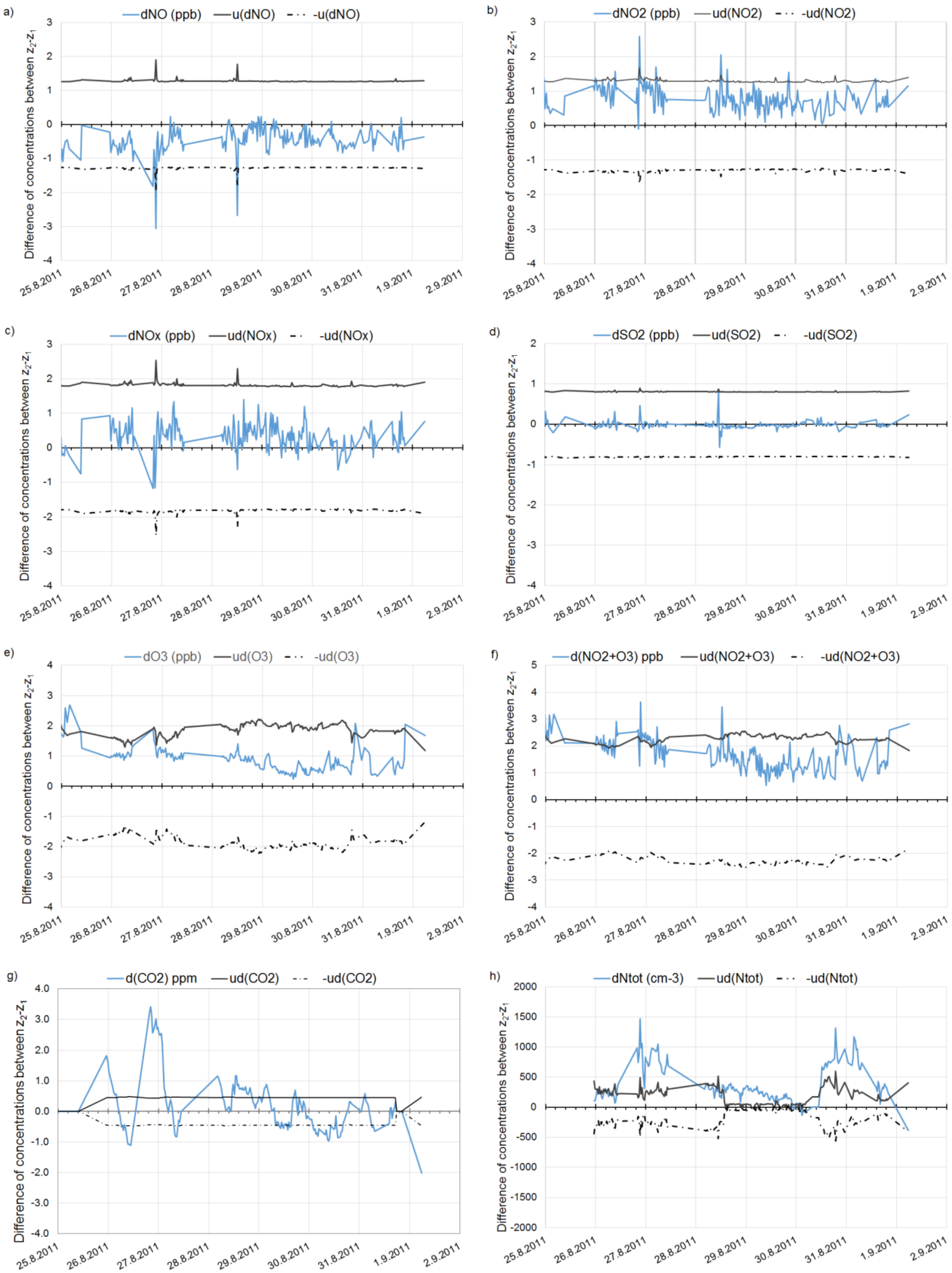

Figure S3. Time series of concentration differences between the measurement heights for gaseous compounds and number concentration of nanoparticles including the uncertainties of the analyzers from Fig. S2. The differences within the uncertainty curves cannot be used for the flux calculations.

Table S1. Estimated relative standard uncertainties u (%) for each of the contributing sources (eq. 12) as well as the relative expanded uncertainty of the fluxes U (%) are presented (see in the text). The fluxes were calculated by the GR method. Sub index 1 refers to the lower and index 2 to the higher measurement height, and S refers to the median concentation over the measurement period. The relative expanded uncertainty is presented in situations of stationary meteorology ($U_{Stat.Met}$) and not stationary meteorology ($U_{Pre.Met}$) during the measure campaigns for CO_2 and Ntot. For the other gases the fluxes were not clearly detectable (Fig. S3).

Uncertainty source	**Uncertainty source**	**Standard uncertainty, u**			**single uncertainties and parameters**		**Weight $(\partial F(x_i)/\partial x_i)^2$**	**Standard uncertainty, *u***
Flux of gases and particles	$Fc = -\frac{ku_*(c(z_2)-c(z_1))}{\left(\ln\left(\frac{z2}{z_1}\right) - \Psi_c(\zeta 2) + \Psi_c(\zeta 1)\right)}$	$\frac{u_c(F_c)^2}{F_c^2} = \frac{u(u_*)^2}{u_*^2} + \frac{u(\Psi_h)^2}{\left(\ln\left(\frac{z_2}{z_1}\right) - \Delta\Psi_h\right)^2} + \frac{u(\Delta c)^2}{\Delta c^2} + \frac{u(z)^2}{\left(\ln\left(\frac{z_2}{z_1}\right) - \Delta\Psi_h\right)^2}\left(\frac{1}{z_1^2}+\frac{1}{z_2^2}\right)$						
Friction velocity	$u_* = \left(\overline{u'w'}\right)^{1/2}$	stationary meteorology, see in text					1.000	**7.0 %**
		non stationary meteorological condition, see in text					1.000	**15.0 %**
Integral function, Ψh	$\Psi h = \int_{\zeta o}^{\zeta}(1-\phi_h(\zeta'))d\zeta'/\zeta'$	$\left(\frac{u(\Delta\Psi)}{\Delta\Psi}\right)^2 = \frac{u(\varphi)^2}{(1-\varphi)^\wedge 2} + [(\frac{1}{\zeta 1})^2+(\frac{1}{\zeta 2})^2]\cdot(\frac{u(\zeta)}{\ln(\frac{\zeta 2}{\zeta 1})})^2$			$u(\phi_h)$	0.10		
					$\phi_{h,ave}$	0.56		
	$\Delta\Psi=(1-\Phi_{h(ave)})\ln(\zeta_2/\zeta_1)$				$u(\phi_h)$	17.1 %	0.222	**26.4 %**
					$\Delta\Psi$	-0.0747		
Stability parameter ζ								
	ζ_1				$u(\zeta_{Z1})$	0.06		
					$\zeta_{Z1,ave}$	-0.07		
	ζ_3				$u(\zeta_{Z2})$	0.07		
					$\zeta_{Z2,ave}$	-0.08		
Measurement height, m	Concentration C_2 at Z_2				z_1(m)	7.2		
	Concentration C_1 at Z_1				z_2(m)	10.7		
		$(z_1^2 + z_2^2)/[z_1 * z_2 * \ln(z_2/z_1)-\Delta\Psi)]^{2*} * u(z)^2$			u_{zm}(cm)	50.0		
					u_{zr}(cm)	75.0		
							0.126	**8.4 %**
Concentration S = CO_2, Ntot			$u(S_{zi})$	$u(S_{zi})$	$u(S_z)$	rel. $u(S_z)$	S_{z1}	S_{z2}
	Carbon dioxide (ppm)	$\left(\frac{u(\Delta S)}{\Delta S}\right)^2 = (u(S_{,2})^2 + (u(S_1)^2$	$u(CO_{2,z2})$	0.800	0.472	**0.1 %**	390	389
			$u(CO_{2,z1})$	0.500				
	Particles, Ntot (# cm^{-3})		$u(N_{tot,z2})$	272.30	341.78	**9.1 %**	3755	4951
			$u(N_{tot,z1})$	206.55				
Wind speed, WS	**Correction of wind speed with CFD calculation**		u(WS(z))				1	**8.90 %**
Expanded uncertainty of flux				**Flux(median)**		**$U_{Stat.Met}$**		**$U_{Prev.Met}$**
	$U(F_{CO2})$			**-0.004**	**mg $m^{-2}s^{-1}$**	**24.9 %**		**36.4 %**
	$U(F_{Ntot})$			**-229.1**	**cm^{-3} m s^{-1}**	**30.8 %**		**40.7 %**

Figure S4 shows the differences on the time averages and respond times during the Harmaja measurement campaign in 2012. In Fig. S4a the time series of the ΔSO_2 and ΔCO_2 concentrations are presented at two different time integration: 15 s and 1 min. The response time of the SO_2 analyzer, Thermo 34 CTL, was improved to 15 s by changing the sample flow rate and shortening the sample tubes inside the analyser. The respond time of the CO_2 analyzer, Picarro G2301, was less than 1s. The calculated FSCs were nearly the same for both cases when the results were obtained from the peak areas. However, the FSC calculated from the peak area value was somewhat higher compared to that of the peak maximum value, in this case 0.46% and 0.40%, respectively. In Fig. S4b the emission peak of CO_2 is illustrated at three different time integration: 1 sec, 15 sec and 1 minute resulting peak area as 34.1 ppm min, 33.25 ppm min, and 33.14 ppm min, respectively. The response time of the analyser defines the shortest integration time of the data collection.

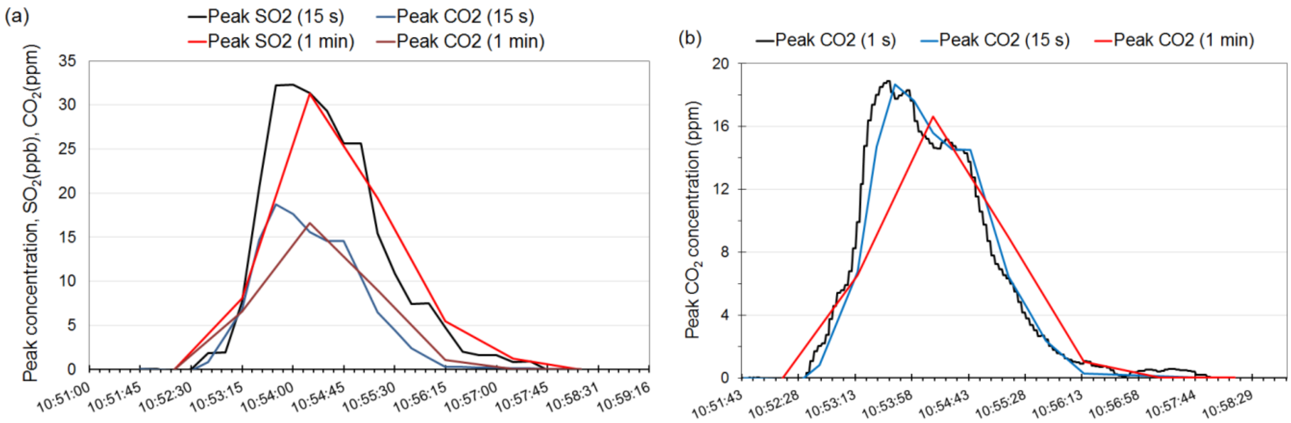

Figure S4. Comparison of the ship emission peak with different time frequency of data collection and response time for SO_2 and CO_2 on the left and CO_2 peak with different time averages on the right. Background concentrations were subtracted.